Key Points:
- The 2015 eruption was the largest and the first on the north rift zone since at least the mid-1980s and the most mafic since ~1450 Common Era
- A change in lava composition followed an increase in the magma supply rate and a decreased repose interval
- At least 11 lava flows with a range of MgO content were fed by a dike >19 km long that tapped a zoned magma body beneath the caldera

Supporting Information:
- Supporting Information S1
- Movie S1

Correspondence to:
W. W. Chadwick,
bill.chadwick@noaa.gov

Voluminous eruption from a zoned magma body after an increase in supply rate at Axial Seamount

W. W. Chadwick Jr[1], J. B. Paduan[2], D. A. Clague[2], B. M. Dreyer[3], S. G. Merle[1], A. M. Bobbitt[1], D. W. Caress[2], B. T. Philip[4], D. S. Kelley[4], and S. L. Nooner[5]

[1]Oregon State University/CIMRS, Hatfield Marine Science Center, Newport, Oregon, USA, [2]Monterey Bay Aquarium Research Institute, Moss Landing, California, USA, [3]Department of Earth and Planetary Sciences, University of Santa Cruz, Santa Cruz, California, USA, [4]School of Oceanography, University of Washington, Seattle, Washington, USA, [5]University of North Carolina at Wilmington, Wilmington, North Carolina, USA

Abstract Axial Seamount is the best monitored submarine volcano in the world, providing an exceptional window into the dynamic interactions between magma storage, transport, and eruption processes in a mid-ocean ridge setting. An eruption in April 2015 produced the largest volume of erupted lava since monitoring and mapping began in the mid-1980s after the shortest repose time, due to a recent increase in magma supply. The higher rate of magma replenishment since 2011 resulted in the eruption of the most mafic lava in the last 500–600 years. Eruptive fissures at the volcano summit produced pyroclastic ash that was deposited over an area of at least 8 km^2. A systematic spatial distribution of compositions is consistent with a single dike tapping different parts of a thermally and chemically zoned magma reservoir that can be directly related to previous multichannel seismic-imaging results.
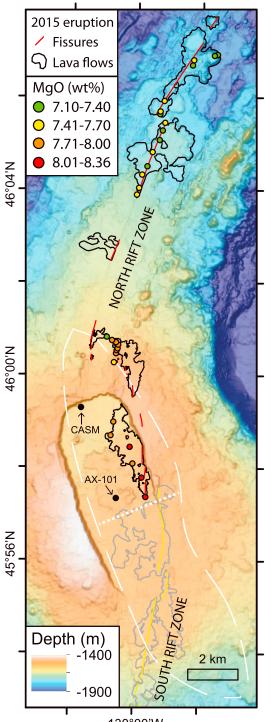
1. Introduction

One of the biggest challenges in volcanology is relating the visible products of eruptions with the hidden subsurface supply systems, storage zones, and conduits that deliver magma to the Earth's surface [*Sigmundsson*, 2006; *Poland et al.*, 2014]. Knowledge of the roots of volcanoes helps us to understand why eruptions occur and the meaning of changes in their character in space and time [*Cashman and Sparks*, 2013]. These relationships are especially cryptic at submarine volcanoes [*Wright et al.*, 2012; *Soule*, 2015], even though submarine volcanoes produce most of Earth's volcanic output [*Crisp*, 1984]. Here we present results from an eruption in 2015 at Axial Seamount that reveals links between an increase in supply to a zoned magma reservoir, dike intrusion into a rift zone, and the composition of new lavas.

Axial Seamount is the most active submarine volcano in the NE Pacific due to its location on the Juan de Fuca spreading ridge (JdFR) [*Embley et al.*, 1990] and its enhanced magma supply from the Cobb hot spot [*Desonie and Duncan*, 1990; *Chadwick et al.*, 2014]. It has a summit caldera and two rift zones that extend to the north and south (Figure 1). The volcano has experienced >50 eruptions in the past 1600 years [*Clague et al.*, 2013a]. Axial Seamount erupted in 1998 and 2011, producing lava flows from the same section of the upper south rift zone (SRZ) along the SE edge of the summit caldera [*Embley et al.*, 1999; *Caress et al.*, 2012; *Chadwick et al.*, 2013]. During both eruptions, magma intruded from a large reservoir beneath the summit [*West et al.*, 2001; *Arnulf et al.*, 2014] as a dike that propagated southward at least 30–50 km along the SRZ. The diking events resulted in eruption of sheet and pillow flows in the caldera and a pillow ridge downrift in 2011; no known downrift eruption occurred in 1998 [*Dziak and Fox*, 1999; *Caress et al.*, 2012; *Chadwick et al.*, 2012]. The April 2015 eruption at Axial Seamount was the first since monitoring and mapping began in the mid-1980s to occur along the north rift zone (NRZ) [*Clague et al.*, 2013a] and the first with data streamed live to shore from the cabled instrument network of the Ocean Observatories Initiative (OOI) [*Kelley et al.*, 2014, 2015].

2. Mapping of the 2015 Lava Flows

Volcanic unrest in 2015 at Axial Seamount began with an increase in seismicity starting at ~04:20 on 24 April (all times in Coordinated Universal Time (UTC)) [*Wilcock et al.*, 2016], followed by the onset of large tilts and rapid deflation in the caldera at ~06:00 [*Nooner and Chadwick*, 2016]. Earthquake epicenters during the first 24 h clustered along the eastern edge of the caldera [*Wilcock et al.*, 2016]. Hydroacoustic (waterborne) impulsive
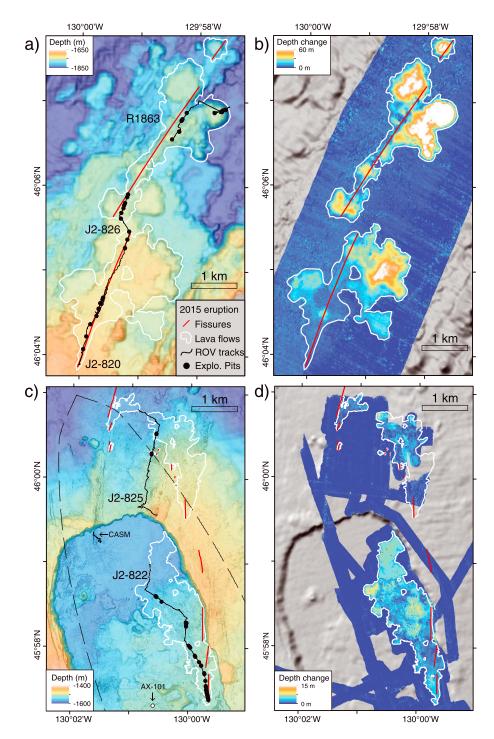
Figure 1. Map of 2015 lava flows (black outlines) and new fissures (red lines) in the summit caldera and on the north rift zone. Also shown are 2011 lava flows (grey outlines) and eruptive fissures (yellow lines) on south rift zone. Lava samples collected by ROV are shown by dots, colored according to their MgO content, showing a northward progression from high to low (see Figure 4). Dashed white outline is magma reservoir from MCS results [*Arnulf et al.*, 2014], with dotted white line separating zones of high melt (south) from crystal mush (north). CASM vent field and benchmark AX-101 are labeled.

signals originating from north of the caldera commenced at ~9:00 and lasted for several weeks [*Wilcock et al.*, 2016]. The source locations of the hydroacoustic signals prompted a bathymetric resurvey of the NRZ and NE summit during the first posteruption expedition to Axial (TN326 in July 2015) using the EM302 multibeam sonar system on board the R/V *Thompson* [*Kelley et al.*, 2015]. Comparisons between this survey and previous EM302 bathymetry collected on the NRZ by the R/V *Thompson* (TN300 in September 2013) revealed seafloor depth changes up to 128 m, located 8–16 km north of the caldera that defined voluminous new lava flows along the NRZ (Figures 1, 2a, 2b, and S1–S3 in the supporting information).

The 2015 EM302 bathymetry was also compared with higher-resolution (1 m) bathymetry collected in 2006–2007 by the Monterey Bay Aquarium Research Institute autonomous underwater vehicle (AUV) *D. Allan B.* in and near the caldera [*Clague et al.*, 2013a]. This comparison revealed additional thinner (<10 m) lava flows on the NE caldera floor and on the north caldera rim, which were mapped at 1 m resolution with the AUV *Sentry* and sampled by the remotely operated vehicle (ROV) *Jason* during TN327 in August 2015 (Figures 1, 2c, 2d, and S4). The 2015 lava flows and eruptive fissures are mapped using a combination of bathymetry, depth differences and ROV dive observations (see supporting information). An additional EM302 survey of Axial Seamount's SRZ during TN327 confirmed that the 2015 eruption was restricted to the summit and NRZ.
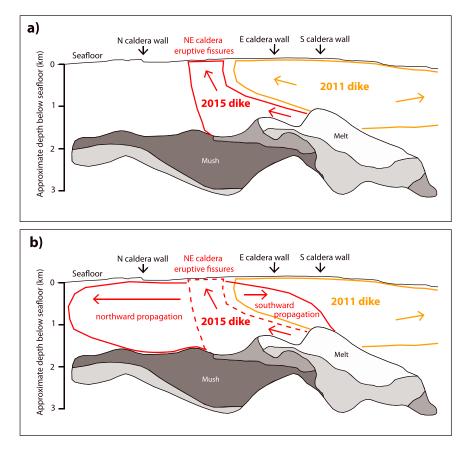
The mapping results show at least 11 separate lava flows erupted from 13 fissures, over a distance

Figure 2. Maps of (a and c) posteruption bathymetry and (b and d) depth changes between preeruption and posteruption surveys, on the north rift zone (Figures 2a and 2b) and at the summit (Figures 2c and 2d). The 2015 lava flow outlines (white), fissures (red lines), ROV dive tracks (black lines), and explosion pits (black dots) are shown. Dashed black outline in Figure 2c is magma reservoir from MCS results [*Arnulf et al.*, 2014].

of 19 km (Figures 1 and S1 and Table S1). The southernmost eight flows are smaller with maximum thicknesses of 5–19 m, whereas the northernmost three flows are up to 67–128 m thick (Figures 2a, 2b, S2, and S3) and represent ~92% of the erupted volume (Table S1). The 2015 flows have a total area of 11.1×10^6 m^2 and a combined volume of 1.48×10^8 m^3 (determined from bathymetric resurveys, see supporting information), which is 50% larger than the volume erupted at Axial Seamount in 2011 (0.99×10^8 m^3)

Figure 3. Sequential cross sections along the east side of the summit caldera at Axial Seamount and multichannel seismic line JF61 of *Arnulf et al.* [2014], showing interpretation of the 2015 dike intrusion. Grey areas are gradients of melt and mush zones within subcaldera magma reservoir as interpreted by *Arnulf et al.* [2014]. Orange lines show extent of 2011 dike along the upper south rift zone. (a) Red lines show initial dike intrusion from the high-melt zone of the magma reservoir feeding the 2015 eruptive fissures in the NE caldera. (b) Subsequent propagation of the 2015 dike shows simultaneous lateral propagation of the dike both northward and southward. The dike did not propagate far to the south nor reach the surface there, because the compressive stresses left over from the 2011 dike intrusion effectively blocked it in that direction. Instead, the 2015 dike continued propagating to the north along the north rift zone.

[*Caress et al.*, 2012; *Chadwick et al.*, 2012] and nearly 5 times the estimated 1998 erupted volume (0.31×10^8 m^3) [*Chadwick et al.*, 2013]. This larger erupted volume and the dramatically decreased recurrence interval (13 years between 1998 and 2011 versus 4 years between 2011 and 2015) are evidence of an increased magma supply at Axial Seamount, consistent with an increased rate of inflation since 2011 detected by geodetic monitoring [*Nooner and Chadwick*, 2016]. The coeruption seismicity [*Wilcock et al.*, 2016] and the lava chemistry (described below) indicate that magma first intruded from the summit reservoir as a dike along the eastern edge of the caldera and then propagated northward into the NRZ after ~07:00 on 24 April (Figure 3); thus, the lava flows likely erupted from south to north.

Mapping of the 2015 eruptive fissures provides new insights into how the summit magma reservoir is linked to the NRZ (Figures 1 and 2). Previously, Axial Seamount's rift zones were envisioned to mimic an overlapping spreading center [*Embley et al.*, 1990], because (a) the SRZ merges with the SE edge of the caldera and (b) the surface expression of the NRZ intersects the north central caldera-bounding fault near the CASM hydrothermal field and extends ~5 km southward across the caldera floor as sparse fissures that intersect the central western caldera wall [*Clague et al.*, 2013a]. However, the 2015 eruption shows that the northward intruding dike in 2015 originated from the same zone along the eastern edge of the caldera as the dikes that propagated southward in 1998 and 2011. This is consistent with recent multichannel seismic (MCS) results [*Arnulf et al.*, 2014] indicating that the underlying magma reservoir is offset to the east compared to the bounding walls of the caldera (Figure 1), perhaps reflecting the continued westward migration of the JdFR with time relative to the Cobb hot spot. The MCS results also suggest that the magma reservoir is zoned from
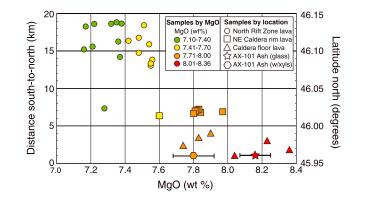
Figure 4. Images from 2015 ROV *Jason* dives: (a) edge of the thin 2015 flow inside the caldera, (b) ash on benchmark AX-101 (see Figure 2c for location), (c) eruptive fissure on NRZ flow, (d) thick NRZ flow blanketed by microbial mat, (e) tube-worms and pandorae worms (*Ridgeia piscesae* and *Paralvinella pandorae*, respectively) at active vent on NRZ lava, and (f) explosion pit in 2015 lava (see also Figure S3).

melt dominated in the southeast to predominantly crystal-rich mush in the northwest, based on the strength of seismic reflections [*Arnulf et al.*, 2014]. The 2015 eruptive fissures extend across this gradient. We interpret that a single dike fed all the 2015 eruptive fissures and that the left-stepping en echelon fissures north of the caldera reflect a clockwise rotation of the near-surface stress field between the caldera and NRZ, directly over the northern tip of the MCS-imaged magma body (Figures 1 and 2c). This interpretation is supported by the smooth and continuous deflation measured during the eruption [*Nooner and Chadwick*, 2016]. Multiple dikes, as interpreted by *Wilcock et al.* [2016], would have likely created interruptions and pauses in the deflation signal.

3. Morphology of the 2015 Lava Flows

The southernmost and northernmost lava flows differ in character and illustrate how the eruption varied temporally and spatially. AUV bathymetry (Figures 2c, 2d, and S4) and ROV dive observations of the southernmost flow in the caldera show that it has mostly lobate sheet morphology with areas of collapse in its interior where lava was channelized in preexisting depressions as it flowed downslope to the north (Figure 4a and Movie S1). The flow is thin (<14 m) with only minor hydrothermal staining and no active venting observed in August 2015, suggesting that it was emplaced rapidly and cooled quickly. A few millimeters of ash were deposited on geodetic benchmarks deployed in 2010 within the caldera (Figure 4b), consisting of bubble-wall shards (limu o Pele) and angular glass fragments that overlap in composition with the caldera flow (Figure 5 and Table S2). This indicates that pyroclastic activity occurred at the nearby 2015 eruptive fissures, and ash was transported at least 2–3.5 km horizontally (based on the presence/absence of ash on the network of 10 benchmarks) by coeruption plumes and prevailing currents [*Clague et al.*, 2009; *Barreyre et al.*,

Figure 5. Plot of MgO versus distance south-to-north and latitude for 2015 lava and ash samples. Symbols are colored according to their MgO content as in Figure 1, and their shape indicates sample type and location. The ash samples are averages of analyses of nine glass particles from benchmark AX-101 (see Figure 2b), with and without microlite crystals (error bars are $\pm 1\sigma$). See also Table S2.

2011]. This is the first confirmed widespread ash deposit from a monitored deep-sea eruption and shows that magmatic degassing can produce low-level fountaining, even at this depth (>1500 m). Ash deposits were not seen on the same benchmarks after the 2011 eruption. These observations are consistent with the higher initial deflation rate in 2015 (a proxy for the rate of magma withdrawal from the summit reservoir and probably eruption rate) compared to 2011 [*Nooner and Chadwick*, 2016].

In contrast, the thick, voluminous lava flows on the NRZ show evidence for longer emplacement and slower cooling. The thick NRZ flows have pillow lava on their steep margins and mixed pillows and lobate morphology in their interiors. The eruptive fissures for the thick flows are marked by linear depressions with lava drainback features in some places (Figure 4c and Movie S1). The thick northern flows were covered over broad areas with a yellow orange microbial "eruption mat" near eruptive fissures and where the flows are >10 m thick. The mat apparently grew, while the flows cooled [*Chadwick et al.*, 2013; *Meyer et al.*, 2013]. Locally, this mat completely blanketed the new flows and nearby older flows (Figure 4d and Movie S1). Active low-temperature hydrothermal venting was observed on the still-cooling thick flows, and some vents had been colonized by tubeworms and pandorae worms, just 4 months after the eruption (Figure 4e and Movie S1).

Numerous pits, 0.5–2 m across and <1 m deep, mark the 2015 lava flows that apparently formed as the result of small steam explosions. The pits are surrounded by angular, broken pieces of the flow's upper crust thrown outward within a radius of a few meters (Figures 4f and S5). These pits occur in lava with pillow or lobate morphology where individual lobes had partially drained under a solid upper crust to form a cavity where seawater could infiltrate and flash to steam, similar to the process envisioned during lava pillar formation [*Chadwick*, 2003; *Perfit et al.*, 2003]. Eighty-seven explosion pits were crossed during ROV transects (Figures 2a, 2c, and S4), but extrapolating from the limited area observed to the total area of the 2015 lava flows suggests there could be thousands of them (see supporting information). The coincidence of the locations of the seismoacoustic signals [*Wilcock et al.*, 2016] with the outlines of the 2015 lava flows is remarkable and strongly suggests that they are directly associated with flow emplacement. Likewise, the duration of the seismoacoustic signals (until 21 May) [*Wilcock et al.*, 2016] is similar to the duration of deflation (until 19 May) [*Nooner and Chadwick*, 2016], suggesting that both record the time that lava was being emplaced on the distal NRZ, considerably longer than the 6 day durations of the two previous eruptions [*Chadwick et al.*, 2012; *Chadwick et al.*, 2013]. The number of impulsive seismic signals peaked early and decreased quasi-exponentially with time [*Wilcock et al.*, 2016], similar to the rate of coeruption deflation [*Nooner and Chadwick*, 2016] and probably eruption rate. We propose that these steam explosions are the probable origin of the thousands of "explosion-like" impulsive acoustic signals detected by the seismometers in the caldera during the eruption [*Wilcock et al.*, 2016]. Explosion pits like these are not unique to the 2015 eruption [*Clague et al.*, 2013b] but have not previously been systematically mapped nor associated with seismoacoustic signals. The relationship is important because such signals could signal the start and end of submarine eruptions.

4. Composition of the 2015 Lava Flows

Chemical analyses of the 2015 lava flows (see supporting information) reveal that the lava composition varies systematically with distance from south to north (Figures 1 and 5 and Table S2). The lava flow in the NE

caldera is the most mafic (MgO up to 8.3%), and the large lava flows on the NRZ are more evolved (MgO down to 7.1%). We interpret that this trend reflects that the 2015 dike tapped different parts of the chemically zoned subcaldera magma reservoir along its length. The southernmost eruptive fissures were rooted in the MCS-imaged high-melt zone of the magma reservoir beneath the SE caldera (Figure 3), where the hottest and most mafic magma is stored [*Clague et al.*, 2013a; *Dreyer et al.*, 2013]. This interpretation is consistent with the coeruption seismicity that showed dike propagation southward into the high-melt zone (south of the 2015 eruptive fissures) early in the sequence, before stalling [*Wilcock et al.*, 2016]. Probably at the same time, the dike also propagated northward into the NRZ and progressively tapped more and more of the mush zone where magmas with slightly lower temperatures and more fractionated compositions resided. The lavas erupted along the NRZ were fed from the northern end of the mush zone. Eruption temperatures calculated from the MgO contents [*Sugawara*, 2000] of the glasses sampled to date vary from 1201°C to 1178°C, perhaps reflecting the range in temperature between the melt and mush zones in the magma reservoir.

The high-MgO lavas erupted in the caldera are the most mafic to have erupted at the summit of Axial Seamount since ~1450 Common Era (C.E.) [*Clague et al.*, 2013a]. Thus, the composition of the 2015 lava flows represents a fundamental change at the volcano, which we interpret reflects the arrival of new magma into the summit reservoir. Previous high-resolution bathymetry combined with geologic mapping, age dating, and geochemical sampling showed that the composition of lavas erupted at the summit of Axial Seamount has been nearly bimodal during the last 1000 years [*Clague et al.*, 2013a; *Dreyer et al.*, 2013]. "Group 1" magmas represent a differentiated transitional-mid-ocean ridge basalt (MORB) that is generally aphyric and has lower MgO (≤7.9%), whereas "Group 2" magmas are more mafic normal-MORB and are mostly plagioclase-phyric to ultraphyric with higher MgO (>7.9%) [*Clague et al.*, 2013a; *Dreyer et al.*, 2013]. Group 2 lavas were erupted between 1220 and 1300 C.E., whereas Group 1 lavas were erupted before 1100 C.E. and have been dominant since ~1600 C.E. The two compositions cannot be explained solely by mixing so each is interpreted as eruptions of separate magmas from discrete melting events in the mantle or melting of slightly different mantle sources [*Dreyer et al.*, 2013]. The 2015 summit lavas have features of both Group 1 and Group 2 lavas. They have higher-MgO concentrations and are slightly phyric like Group 2 lavas, but they also have the transitional-MORB composition of Group 1 lavas erupted since ~1600 C.E. Thus, the higher temperatures of the 2015 melts are consistent with the arrival of a new, hot magma from the mantle, but from a source region that is compositionally unchanged during the last ~400 years. This change in lava composition is likely directly related to the fourfold increase in the rate of inflation (and therefore magma supply) measured since 2011 [*Nooner and Chadwick*, 2016] that also decreased the magma residence time. Axial Seamount may be moving into a period of larger and more frequent eruptions of hotter, more mafic lavas.

5. Conclusions

The 2015 eruption at Axial Seamount is remarkable because the location, volume, composition, and morphology of the lava flows can be related to coeruption deformation and seismicity for the first time in a mid-ocean ridge setting because of the new OOI cabled observatory. In addition, the 3-D geometry of the seismically imaged magma body and changes in the magma supply can be linked to changes in the geochemistry, volume, and frequency of erupted lavas and the structures that deliver magma to the surface. Such direct links between processes in the source region of melts in the mantle, the storage zone of magma in the shallow crust, and the character of lavas erupted at the surface reveal that fundamental changes in the magmatic system of a mid-ocean ridge volcano can occur on the time scale of a single eruption cycle. It also suggests that high-melt zones in seismically imaged magma reservoirs are where melt has most recently been delivered and are where eruptions are most likely to be initiated.

References

Arnulf, A. F., A. J. Harding, G. M. Kent, S. M. Carbotte, J. P. Canales, and M. R. Nedimovic (2014), Anatomy of an active submarine volcano, *Geology*, *42*, 655–658, doi:10.1130/G35629.1.

Barreyre, T., S. A. Soule, and R. A. Sohn (2011), Dispersal of volcaniclasts during deep-sea eruptions: settling velocities and entrainment in buoyant seawater plumes, *J. Volcanol. Geotherm. Res.*, *205*, 84–93, doi:10.1016/j.jvolgeores.2011.05.006.

Caress, D. W., D. A. Clague, J. B. Paduan, J. Martin, B. Dreyer, W. W. Chadwick Jr., A. Denny, and D. S. Kelley (2012), Repeat bathymetric surveys at 1-metre resolution of lava flows erupted at Axial Seamount in April 2011, *Nat. Geosci.*, *5*, 483–488, doi:10.1038/NGEO1496.

Cashman, K. V., and R. S. J. Sparks (2013), How volcanoes work: A 25 year perspective, *Geol. Soc. Am. Bull.*, *125*, 664–690, doi:10.1130/B30720.1.

Chadwick, J., R. Keller, G. Kamenov, G. Yogodzinski, and J. Lupton (2014), The Cobb hot spot: HIMU-DMM mixing and melting controlled by a progressively thinning lithospheric lid, *Geochem. Geophys. Geosyst.*, *15*, 3107–3122, doi:10.1002/2014GC005334.

Chadwick, W. W., Jr. (2003), Quantitative constraints on the growth of submarine lava pillars from a monitoring instrument that was caught in a lava flow, *J. Geophys. Res.*, *108*, 2534, doi:10.1029/2003JB002422.

Chadwick, W. W., Jr., S. L. Nooner, D. A. Butterfield, and M. D. Lilley (2012), Seafloor deformation and forecasts of the April 2011 eruption at Axial Seamount, *Nat. Geosci.*, *5*, 474–477, doi:10.1038/NGEO1464.

Chadwick, W. W., Jr., et al. (2013), The 1998 eruption of Axial Seamount: New Insights on submarine lava flow emplacement from high-resolution mapping, *Geochem. Geophys. Geosyst.*, *14*, 3939–3968, doi:10.1002/ggge20202.

Clague, D. A., J. B. Paduan, and A. S. Davis (2009), Widespread strombolian eruptions of mid-ocean ridge basalt, *J. Volcanol. Geotherm. Res.*, 171–188, doi:10.1016/j.jvolgeores.2008.1008.1007.

Clague, D. A., et al. (2013a), Geologic history of the summit of Axial Seamount, Juan de Fuca Ridge, *Geochem. Geophys. Geosyst.*, *14*, 4403–4443, doi:10.1002/ggge.20240.

Clague, D. A., R. A. Portner, B. P. Paduan, and B. M. Dreyer (2013b), Fluidal deep-sea volcanic ash as an indicator of explosive volcanism, Abstract V33H-08 presented at Fall Meeting, AGU, San Francisco, Calif., 9–13 Dec.

Crisp, J. A. (1984), Rates of magma emplacement and volcanic output, *J. Volcanol. Geotherm. Res.*, *20*, 177–211.

Desonie, D. L., and R. A. Duncan (1990), The Cobb-Eickelberg seamount chain: Hotspot volcanism with mid-ocean ridge basalt affinity, *J. Geophys. Res.*, *95*, 12,697–12,712, doi:10.1029/JB095iB08p12697.

Dreyer, B. M., D. A. Clague, and J. B. Gill (2013), Petrological variability of recent magmatism at Axial Seamount summit, Juan de Fuca Ridge, *Geochem. Geophys. Geosyst.*, *14*, 4306–4333, doi:10.1002/ggge.20239.

Dziak, R. P., and C. G. Fox (1999), The January 1998 earthquake swarm at Axial Volcano, Juan de Fuca Ridge: Hydroacoustic evidence of seafloor volcanic activity, *Geophys. Res. Lett.*, *26*(23), 3429–3432, doi:10.1029/1999GL002332.

Embley, R. W., K. M. Murphy, and C. G. Fox (1990), High resolution studies of the summit of Axial Volcano, *J. Geophys. Res.*, *95*, 12,785–12,812, doi:10.1029/JB095iB08p12785.

Embley, R. W., W. W. Chadwick Jr., D. Clague, and D. Stakes (1999), The 1998 Eruption of Axial Volcano: Multibeam anomalies and seafloor observations, *Geophys. Res. Lett.*, *26*(23), 3425–2428, doi:10.1029/1999GL002328.

Kelley, D. S., J. R. Delaney, and S. K. Juniper (2014), Establishing a new era of submarine volcanic observatories: Cabling Axial Seamount and the Endeavour Segment of the Juan de Fuca Ridge, *Mar. Geol.*, *352*, 426–450, doi:10.1016/j.margeo.2014.03.010.

Kelley, D. S., J. R. Delaney, W. W. Chadwick, Jr., B. Philip, and S. G. Merle (2015), Axial Seamount 2015 eruption: A 127-m thick, microbially-covered lava flow, Abstract OS41B-08 presented at 2015 Fall Meeting, AGU, San Francisco, Calif., 14–18 Dec.

Meyer, J. L., N. H. Akerman, G. Proskurowski, and J. A. Huber (2013), Microbiological characterization of post-eruption "snowblower" vents at Axial Seamount, Juan de Fuca Ridge, *Front. Microbiol.*, *4*, 153, doi:10.3389/fmicb.2013.00153.

Nooner, S. L., and W. W. Chadwick Jr. (2016), Inflation-predictable behavior and co-eruption deformation at Axial Seamount, *Science*, doi:10.1126/science.aah4666, in press.

Perfit, M. R., J. R. Cann, D. J. Fornari, J. L. Engels, D. K. Smith, W. I. Ridley, and M. H. Edwards (2003), Interaction of sea water and lava during submarine eruptions at mid-ocean ridges, *Nature*, *426*, 62–65.

Poland, M. P., A. Miklius, and E. K. Montgomery-Brown (2014), Magma supply, storage, and transport at shield-stage Hawaiian volcanoes, in Characteristics of Hawaiian volcanoes, edited by M. P. Poland, T. J. Takahashi, and C. Landowski, U,S, *Geol. Surv. Prof. Pap.*, *1801*, 179–236.

Sigmundsson, F. (2006), *Iceland Geodynamics: Crustal Deformation and Divergent Plate Tectonics*, 209 pp., Springer, Chichester, U. K.

Soule, S. A. (2015), Mid-ocean ridge volcanism, in *Encyclopedia of Volcanoes, edited by H. Sigurdsson*, B. Houghton, H. Rymer, J. Stix and S. McNutt, 2nd ed., pp. 395–403, Academic Press, San Diego, Calif.

Sugawara, T. (2000), Empirical relationships between temperature, pressure, and MgO content in olivine and pyroxene saturated liquid, *J. Geophys. Res.*, *105*(B4), 8457–8472, doi:10.1029/2000JB900010.

West, M. E., W. Menke, M. Tolstoy, S. Webb, and R. Sohn (2001), Magma storage beneath Axial Volcano on the Juan de Fuca mid-ocean ridge, *Nature*, *413*, 833–836.

Wilcock, W. S. D., M. Tolstoy, F. Waldhauser, C. Garcia, Y. J. Tan, D. R. Bohnenstiehl, J. Caplan-Auerbach, R. P. Dziak, A. F. Arnulf, and M. Mann (2016), Seismic constraints on caldera dynamics from the 2015 Axial Seamount eruption, *Science*, doi:10.1126/science.aah5563, in press.

Wright, T. J., et al. (2012), Geophysical constraints on the dynamics of spreading centres from rifting episodes on land, *Nat. Geosci.*, *5*, 242–250, doi:10.1038/ngeo1428.